Supporting Information of

Anthropogenic climate change has changed frequency of past flood during 2010-2013

Yukiko Hirabayashi[1],
Corresponding author
Email: hyukiko@shibaura-it.ac.jp

Haireti Alifu[1]
Email: haireti.alifu.f4@sic.shibaura-it.ac.jp

Dai Yamazaki[2]
Email: yamadai@rainbow.iis.u-tokyo.ac.jp

Yukiko Imada[3]
Email: yimada@mri-jma.go.jp

Hideo Shiogama[4]
Email: shiogama.hideo@nies.go.jp

Yuki Kimura[5]
Email: yuuki.kimura@ms-ad-hd.com

(Institutional addresses)
[1] Department of Civil Engineering, Shibaura Institute of Technology, 3-7-5 Toyosu, Koto-ku, Tokyo 135-8548, Japan.
[2] Institute of Industrial Science, The University of Tokyo, 4 Chome-6-1 Komaba, Meguro City, Tokyo 153-8505, Japan.
[3] Meteorological Research Institute, 1-1 Nagamine, Tsukuba, Ibaraki 305-0052, Japan.
[4] National Institute for Environmental Studies, 16-2 Onogawa, Tsukuba, Ibaraki 305-0053, Japan.
[5] Corporate Planning Department, MS&AD InterRisk Research & Consulting, Inc., 2-105, Kanda Awajicho, Chiyoda-ku, Tokyo 101-0063, Japan

S1 Event attribution experiments

A large-ensemble climate experiment was conducted using an atmospheric general circulation model (AGCM) ,—MIROC5 (Watanabe et al., 2010) —, driven by sea surface temperature (SST), sea ice, and historical external forcing factors. Three types of experiments were performed in this study (Table 1). ALL-LNG (ALL forcing LoNG period runs) is ten-member ensemble run of the AGCM driven by observed SST, sea ice, and historical anthropogenic (i.e., greenhouse gas concentration, sulfate and carbon aerosols, tropospheric and stratospheric ozone, and land use changes) and natural (i.e., solar irradiance changes and large volcanic activity) external forcing between 1949 and 2013. The 100- member ensemble runs of ALL (ALL forcing run) were produced with the same anthropogenic and natural external conditions as the ALL-LNG runs. NAT (NATural forcing runs) is a 100-member ensemble run produced under natural external conditions. Two types of large-ensemble run were integrated for 2010-2013 (Table 1).

The anthropogenic external forcing factors were fixed at the year 1850 and anthropogenic signals were removed from the observed SST and sea ice data. To analyze the uncertainties in removing anthropogenic signals from SST and sea ice data, two NAT experiments (NAT-dtr and NAT-cmip5) were used for the analysis. NAT-dtr calculated anthropogenic SST anomalies based on observed historical trends, whereas NAT-cmip5 used SST differences between the historical and natural-forcing runs of the CMIP5 ensemble (Shiogama et al., 2014). The anthropogenic signals in sea ice were estimated based on the empirical linear relationships between the observed SST and sea ice. The ALL and NAT experiments were used to evaluate the influences of anthropogenic radiation changes on the probability of flood events between 2010 and 2013. Due to the availability of observed external forcing at the time of the experiment, the Representative Concentration Pathway 4.5 scenario was used for external forcing for the period 2006-2011. A previous study using the experiment successfully explained changes in probabilities of the 2010 drought (Shiogama et al., 2013) and 2012 flood in the Amazon region (Kimura et al., 2016).

S2 Selection of historical flood events between 2010 and 2013

Large historical flood events that occurred between 2010 and 2013, the same time period as the event attribution climate experiment, were selected. First, the years and locations of large floods were extracted from the Emergency Events Database (EM-DAT), news media, or stream gauges. Flood events in the EM-DAT with a certain amount of reported damage in the "flood" category were selected, and latitude/longitude coordinates were specified using the reported names of the rivers or cities affected. Stream gauge data from the Global Runoff Data Center (GRDC) from basins with an area > 100,000 km^2 that corresponded to the flood event were then analyzed, and the location and year were determined if the observed annual maximum daily discharge of that year exceeded the magnitude of a 10-year flood (flood with probability of 10% from long-term records). Events selected from EM-DAT or stream gauge data were searched for using the following key words: year and names of rivers or cities. The locations and target years were confirmed with additional data sources (websites and news media) and the main causes of these flood events were investigated. Finally, 22 flood events were selected (Table 2).

The main causes of the flood events were investigated using information from the news media, the season of the occurrence of flood events, and studies related to the events. The most common cause of flooding was heavy rainfall, which was the main cause in 13 of 22 events and the second cause in three events. Eight flood events due to snowmelt and one caused by a storm were also selected.

S3 Extreme distribution function

The frequency of floods corresponding to the magnitude of discharge with a 10-year return period was estimated from the time series of the annual maximum daily discharge by fitting the Gumbel distribution (Gumbel, 1941). The parameters for the distribution function were estimated from the probability-weighted moments (Hosking, 1990) following a similar method described previously (Hirabayashi et al., 2013). For the observed and reanalysis discharge, all available data samples were used to calculate the parameters of the Gumbel probability distribution function, whereas ten ensembles of annual maximum daily discharge for 1949-2013 in the ALL-LNG experiment were used to calculate parameters of the distribution function of climate experiments. Using the parameters obtained from ALL-LNG, the return periods at the location and year of the annual maximum daily discharge were calculated for ALL and NAT (NAT-dtr and NAT-cmip5), respectively.

References:

Gumbel, E. J., 1941, The Return Period of Flood Flows: The Annals of Mathematical Statistics, v. 12, p. 163-190.

Hirabayashi, Y., R. Mahendran, S. Koirala, L. Konoshima, D. Yamazaki, S. Watanabe, H. Kim, and S. Kanae, 2013, Global flood risk under climate change: Nature Climate Change, v. 3, p. 816-821.

Hosking, J. R. M., 1990, L‐Moments: Analysis and Estimation of Distributions Using Linear Combinations of Order Statistics: Journal of the Royal Statistical Society: Series B (Methodological), v. 52, p. 105-124.

Kimura, Y., M. Tanoue, Y. Imada, and Y. Hirabayashi, 2016, An event attribution of the 2012 Amazon flood: Journal of Japan Society of Civil Engineers, Ser. G (Environmental Research), v. 72, p. I_1-I_6.

Shiogama, H., M. Watanabe, Y. Imada, M. Mori, M. Ishii, and M. Kimoto, 2013, An event attribution of the 2010 drought in the South Amazon region using the MIROC5 model: Atmospheric Science Letters, v. 14, p. 170-175.

Shiogama, H., M. Watanabe, Y. Imada, M. Mori, Y. Kamae, M. Ishii, and M. Kimoto, 2014, Attribution of the June-July 2013 Heat Wave in the Southwestern United States: Sola, v. 10, p. 122-126.

Watanabe, M., T. Suzuki, R. O'Ishi, Y. Komuro, S. Watanabe, S. Emori, T. Takemura, M. Chikira, T. Ogura, M. Sekiguchi, K. Takata, D. Yamazaki, T. Yokohata, T. Nozawa, H. Hasumi, H. Tatebe, and M. Kimoto, 2010, Improved Climate Simulation by MIROC5. Mean States, Variability, and Climate Sensitivity: Journal of Climate, v. 23, p. 6312-6335.

Table S1. Summary of selected flood events between 2010 and 2013. The effects of anthropogenic climate change on flood events (E, enhanced; S, suppressed; N/A, no significant effect) were judged as E (S) when both percentile of fraction of attribution (FAR_{50}) scores between ALL and NAT_dtr (dtr) and those between ALL and NAT_CMIP5 (CMIP5) show the same signal.

	River	GRDC	Year	Causes	FAR dtr percentiles			FAR CMIP5 percentiles			Effect
					10th	50th	90th	10th	50th	90th	
1	Mackenzie	4208005	2012	SM, HR	0.17	0.44	0.67	-0.68	-0.17	0.24	N/A
2	Peace	4208450	2011	HR	-0.42	0.14	0.49	-0.94	-0.29	0.18	N/A
3	Fraser	4207900	2012	SM	0.08	0.36	0.58	-0.52	0.01	0.37	E
4	Saskatchewan	4213400	2013	HR	-0.34	0.11	0.42	-0.75	-0.11	0.35	N/A
5	Red	4213573	2011	SM	-1.97	-0.92	-0.26	-1.22	-0.49	0.01	S
6	Missouri	4121801	2011	SM	-1.01	-0.3	0.17	-0.7	-0.07	0.37	S
7	Mississippi	4127501	2011	SM, S	-1.20	-0.29	0.27	-1.48	-0.46	0.13	S
8	Magdalena	3103450	2011	HR	0.16	0.46	0.67	-0.02	0.3	0.52	E
9	Amazon	3623100	2012	HR	0.24	0.45	0.62	0.24	0.48	0.65	E
10	Sava	6545101	2010	SM, HR	-0.54	0.09	0.5	-0.17	0.36	0.69	E
11	Danube	6542100	2013	HR	-0.61	-0.01	0.38	-0.19	0.28	0.62	N/A
12	Kuban	6983350	2012	S	0.31	0.65	0.86	-1.00	-0.24	0.28	N/A
13	Volga	6977100	2012	SM	0.01	0.27	0.48	0.12	0.35	0.52	E
14	Lena	2903429	2010	SM	-0.58	-0.07	0.32	-0.58	-0.12	0.24	S
15	Amur	2906700	2013	HR	0.25	0.54	0.75	0.15	0.45	0.66	E
16	Songhua	2106500	2013	HR	0.37	0.63	0.8	0.17	0.48	0.71	E
17	Yalu	2876500	2010	HR	-0.34	0.16	0.49	-0.84	-0.14	0.32	N/A
18	Indus	2335950	2010	HR	-0.27	0.2	0.52	-0.31	0.17	0.48	E
19	Fitzroy	5101301	2010	HR	-1.47	-0.09	0.64	-1.30	-0.39	0.47	S
20	Murrumbidge, Murray	5204106	2012	HR	-0.14	0.35	0.69	-1.06	-0.33	0.17	N/A
21	Niger	1234150	2010	HR	-0.94	-0.15	0.37	-3.66	-1.84	-0.72	S
22	Okavango	1257100	2011	HR	0.22	0.61	0.81	-1.15	-0.17	0.37	N/A

Note: AF, Africa; AS, Asia; EU, Europe; SA, South America; NA, North America; OC, Oceania;

N/A, not available; HR, Heavy rain; SM, Snow melt; S, Storm.

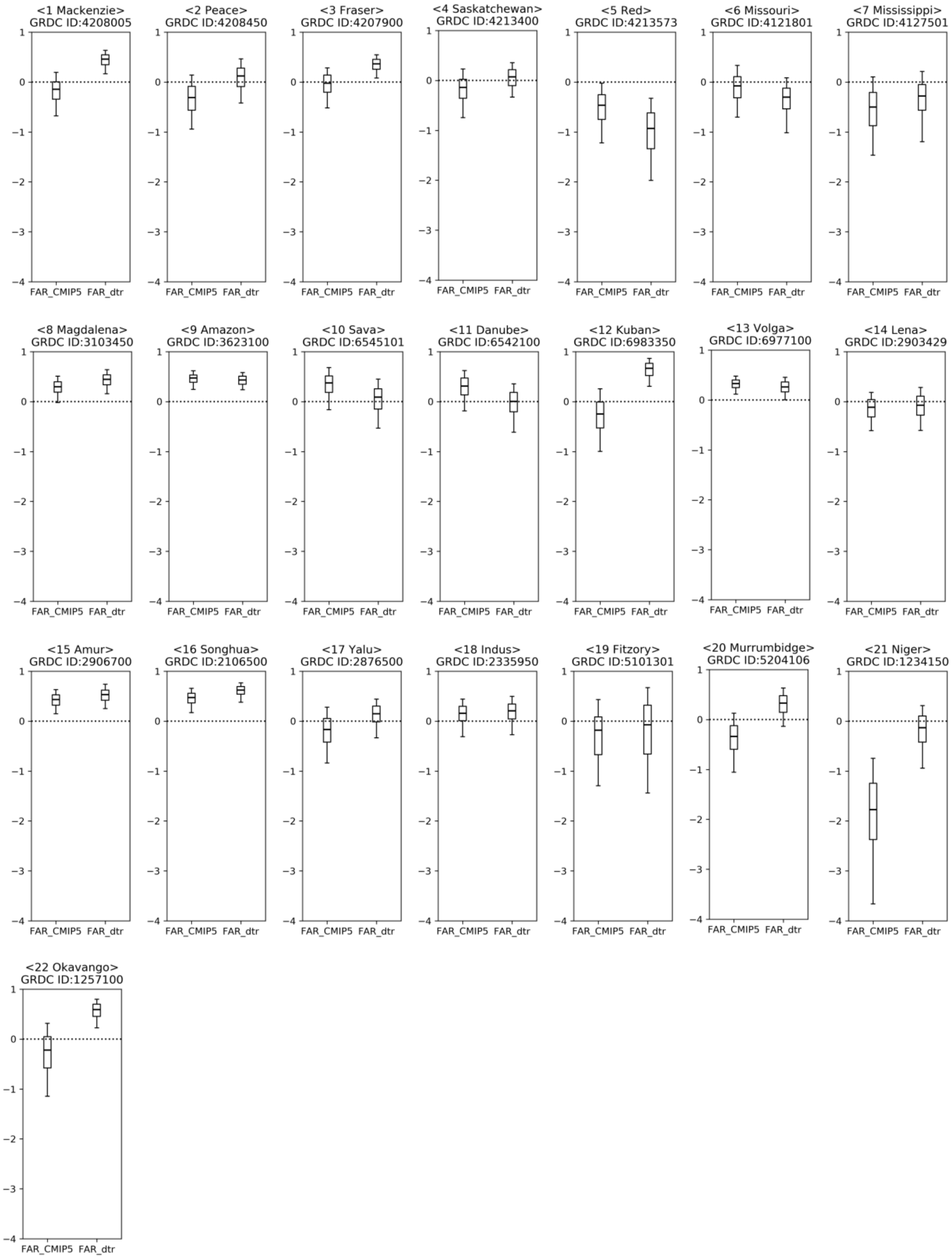

Fig. S1 Results of the evaluation of the fraction of attribution risk based on a bootstrap method.

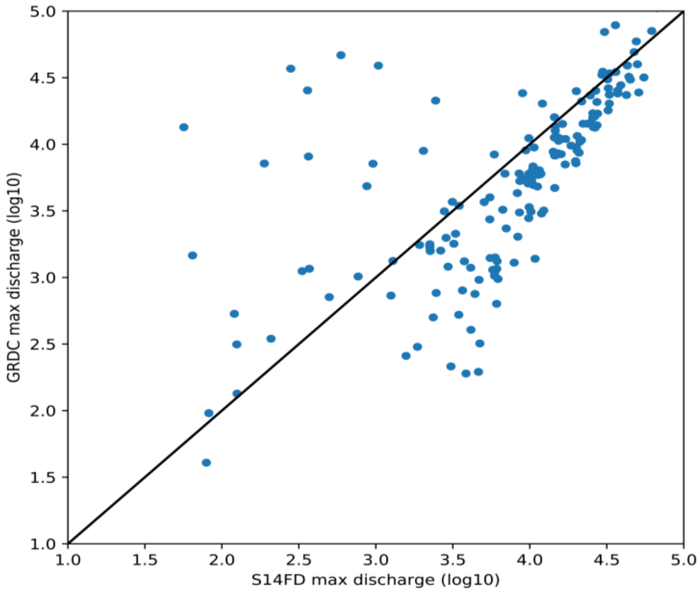

Fig. S2. Scatter plot of the annual maximum discharge derived from GRDC and global daily discharge reanalysis based on the 136 GRDC stations. Geographic location of the stations are shown in Fig. S3.

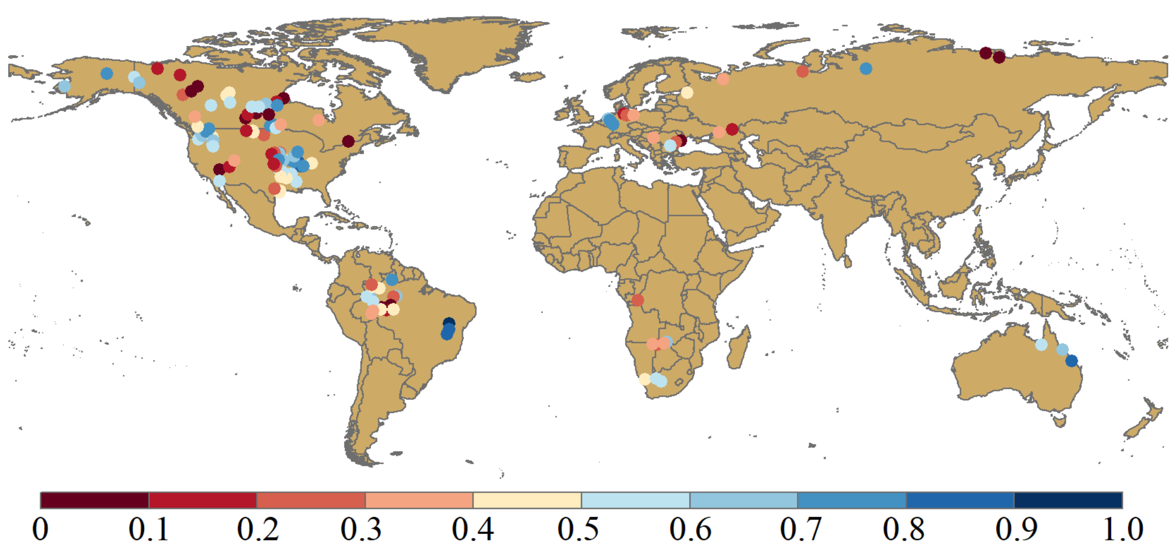

Fig. S3. Correlation of annual max discharge derived from GRDC and global daily discharge reanalysis at 136 GRDC stations.

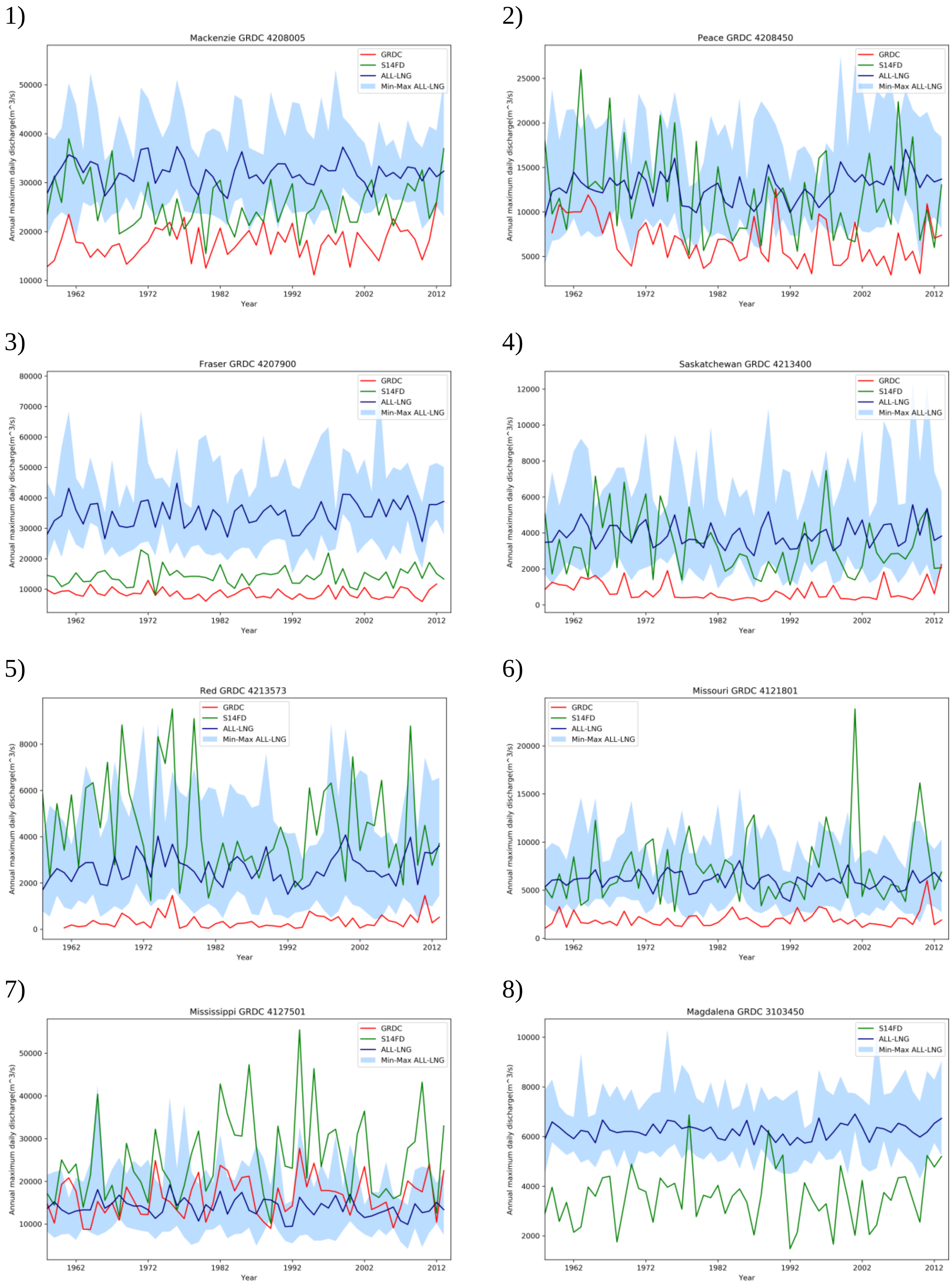

Fig. S4 Comparisons of the annual maximum daily discharge derived from observations (GRDC), discharge reanalysis (S14FD), and ALL-LNG experiments.

9)

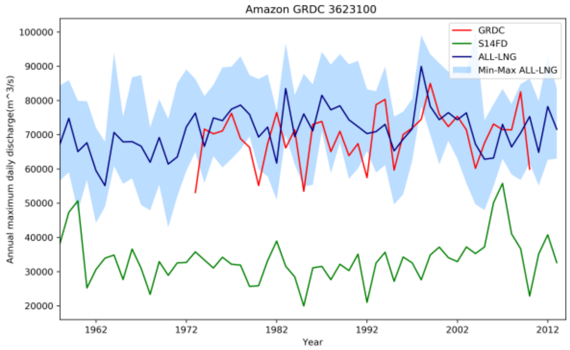

10)

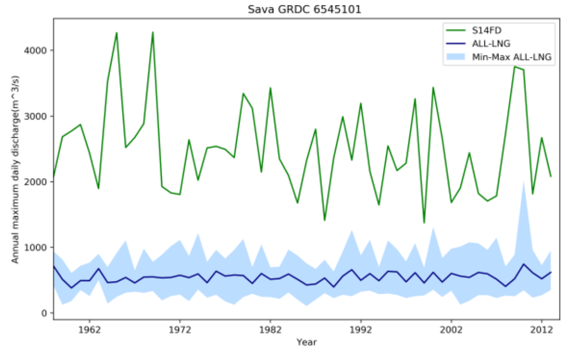

11)

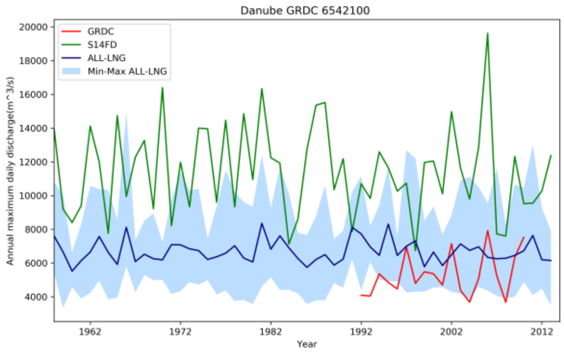

12)

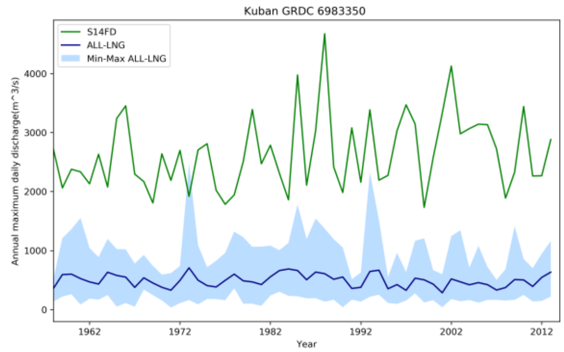

13)

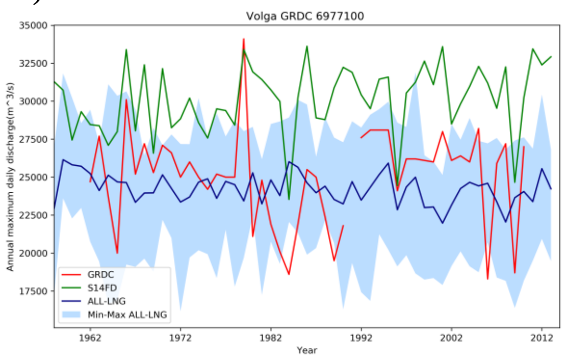

14)

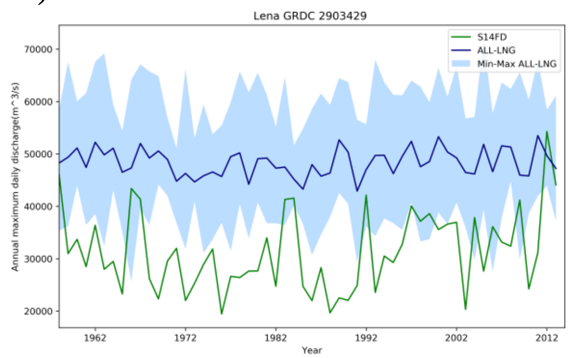

15)

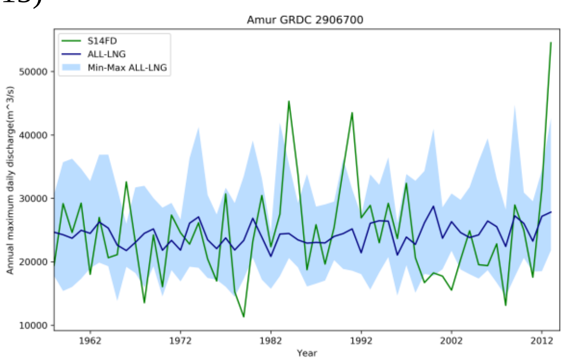

16)

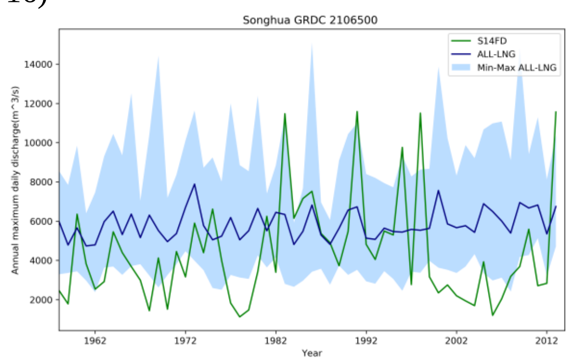

Fig. S4 Comparisons of the annual maximum daily discharge derived from observations (GRDC), discharge reanalysis (S-14FD), and ALL-LNG experiments (continue…)

17)

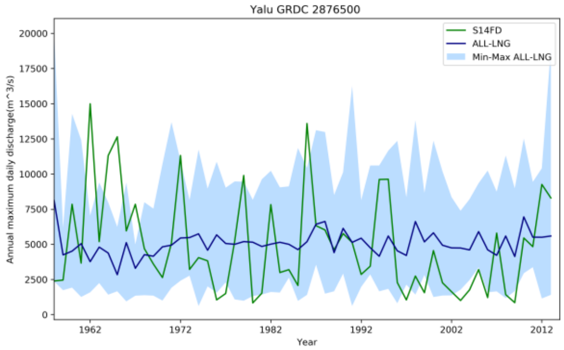

18)

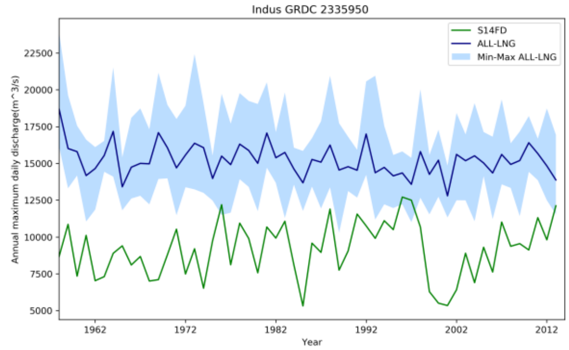

19)

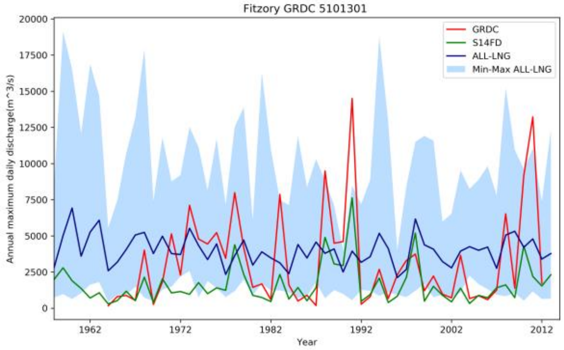

20)

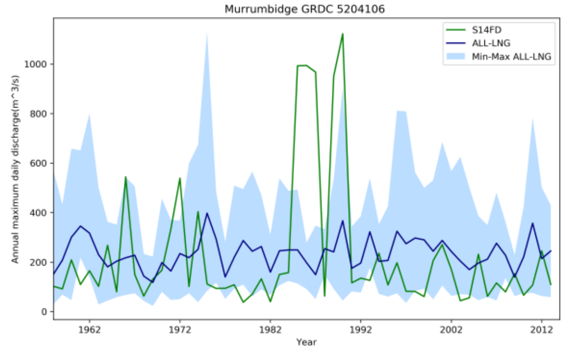

21)

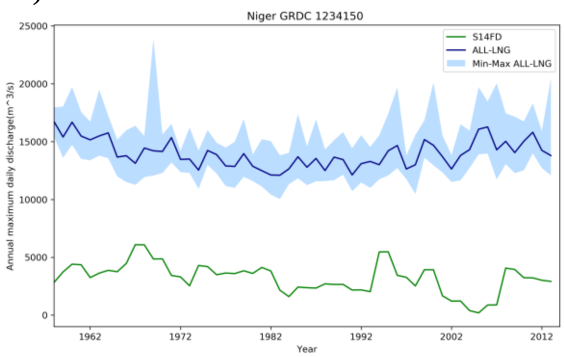

22)

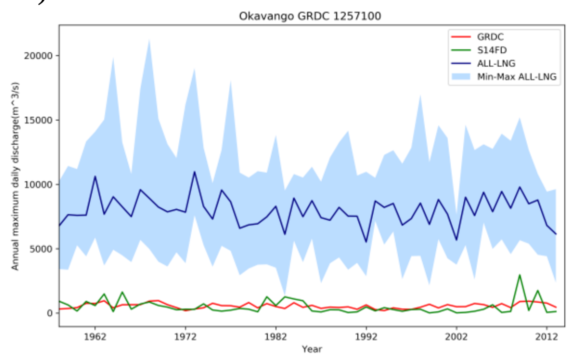

Fig. S4 Comparisons of the annual maximum daily discharge derived from observations (GRDC), discharge reanalysis (S14FD), and ALL-LNG experiments (continue…)

1)

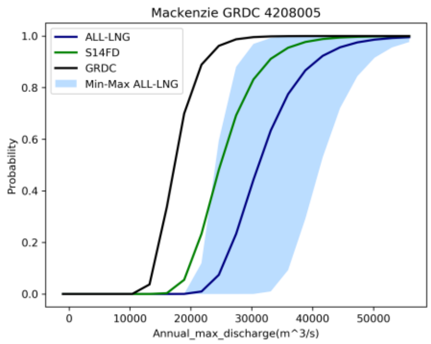

2)

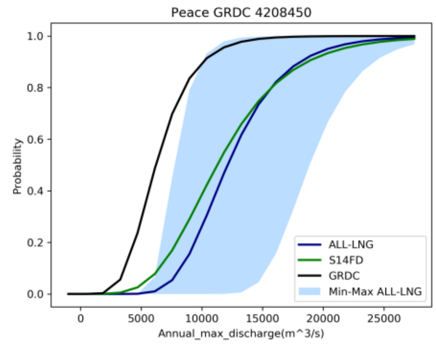

3)

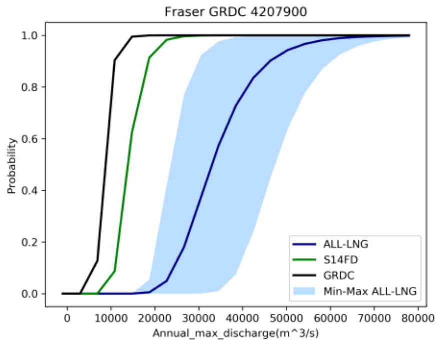

4)

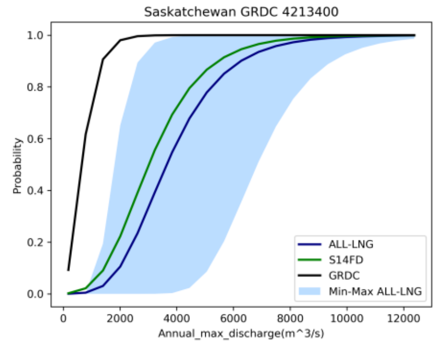

5)

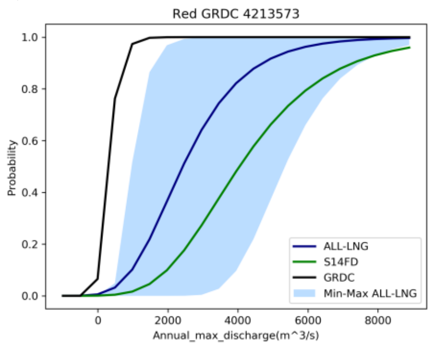

6)

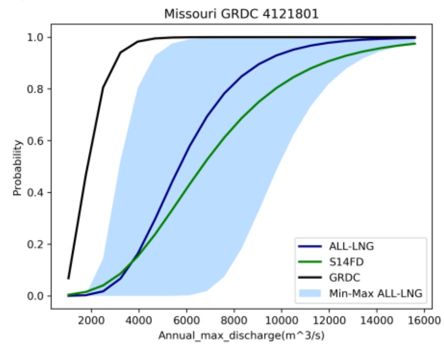

7)

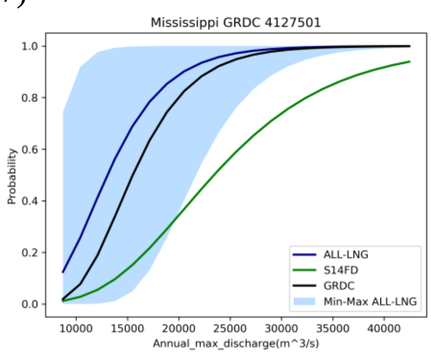

8)

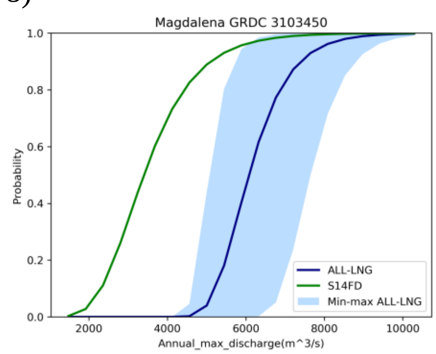

Fig. S5 The cumulative distribution function of annual maximum daily discharge for 22 events derived from observations (GRDC), discharge reanalysis (S14FD), and ALL-LNG experiments. Shade indicates maximum and minimum range among 650 ALL-LNG experiments.

9)

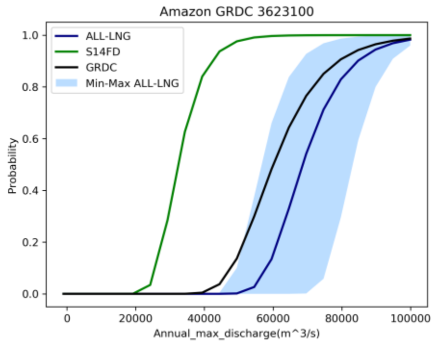

10)

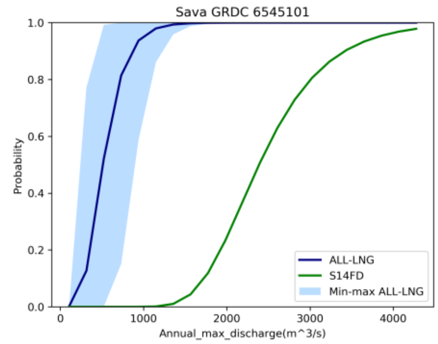

11)

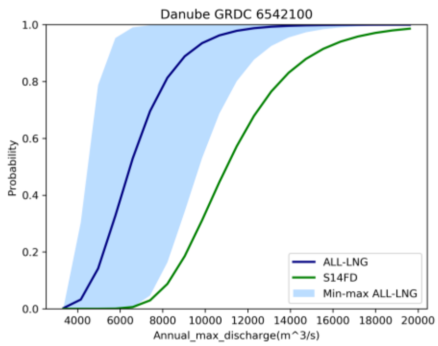

12)

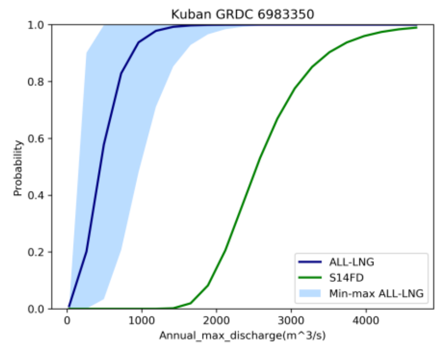

13)

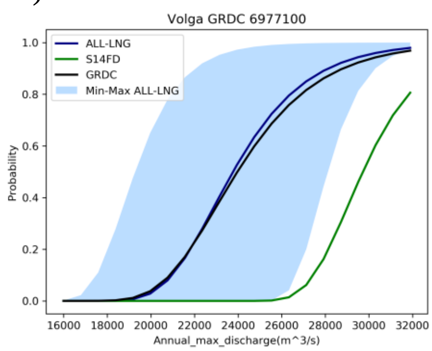

14)

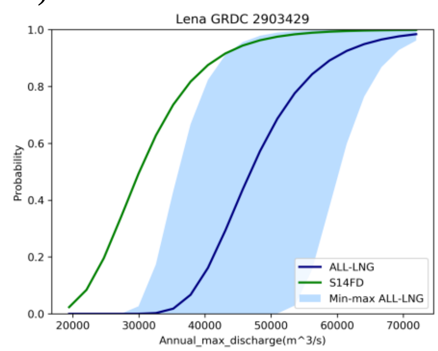

15)

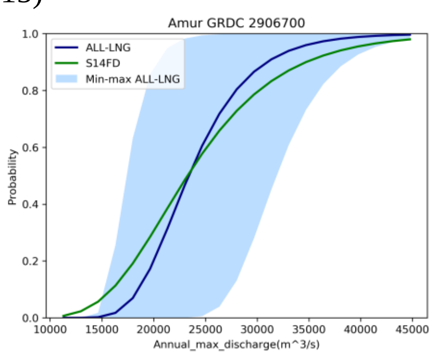

16)

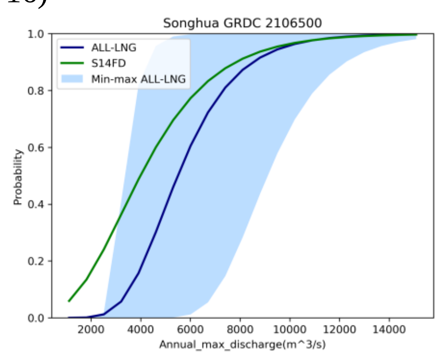

Fig. S5 The cumulative distribution function of annual maximum daily discharge for 22 events derived from observations (GRDC), discharge reanalysis (S14FD), and ALL-LNG experiments. Shade indicates maximum and minimum range among 650 ALL-LNG experiments (continue…).

17)

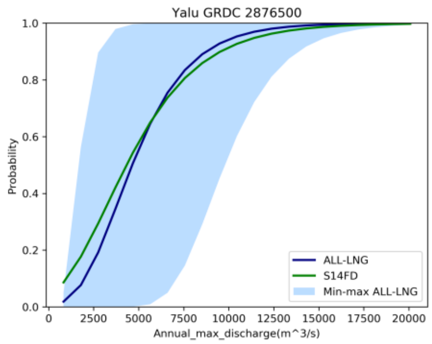

18)

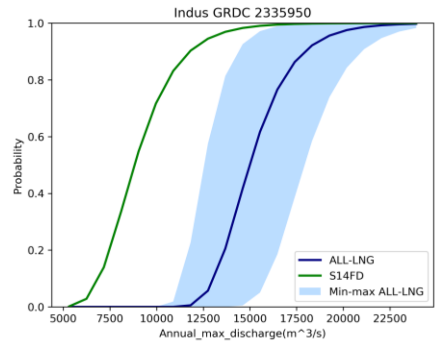

19)

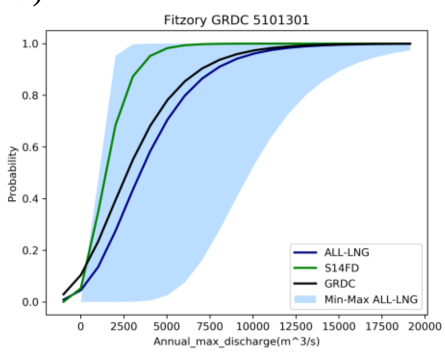

20)

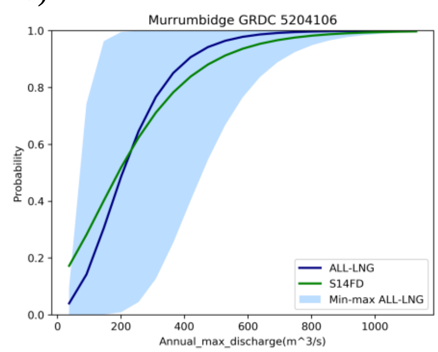

21)

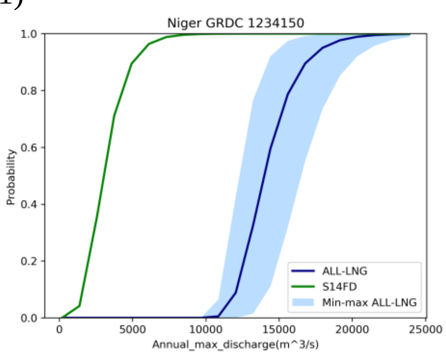

22)

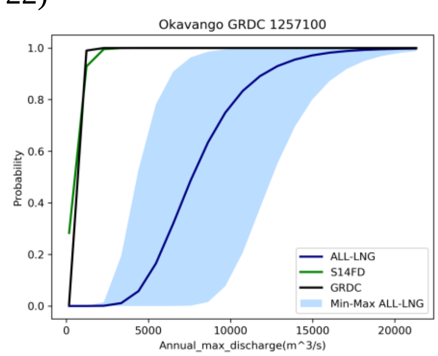

Fig. S5 The cumulative distribution function of annual maximum daily discharge for 22 events derived from observations (GRDC), discharge reanalysis (S14FD), and ALL-LNG experiments. Shade indicates maximum and minimum range among 650 ALL-LNG experiments (continue…).

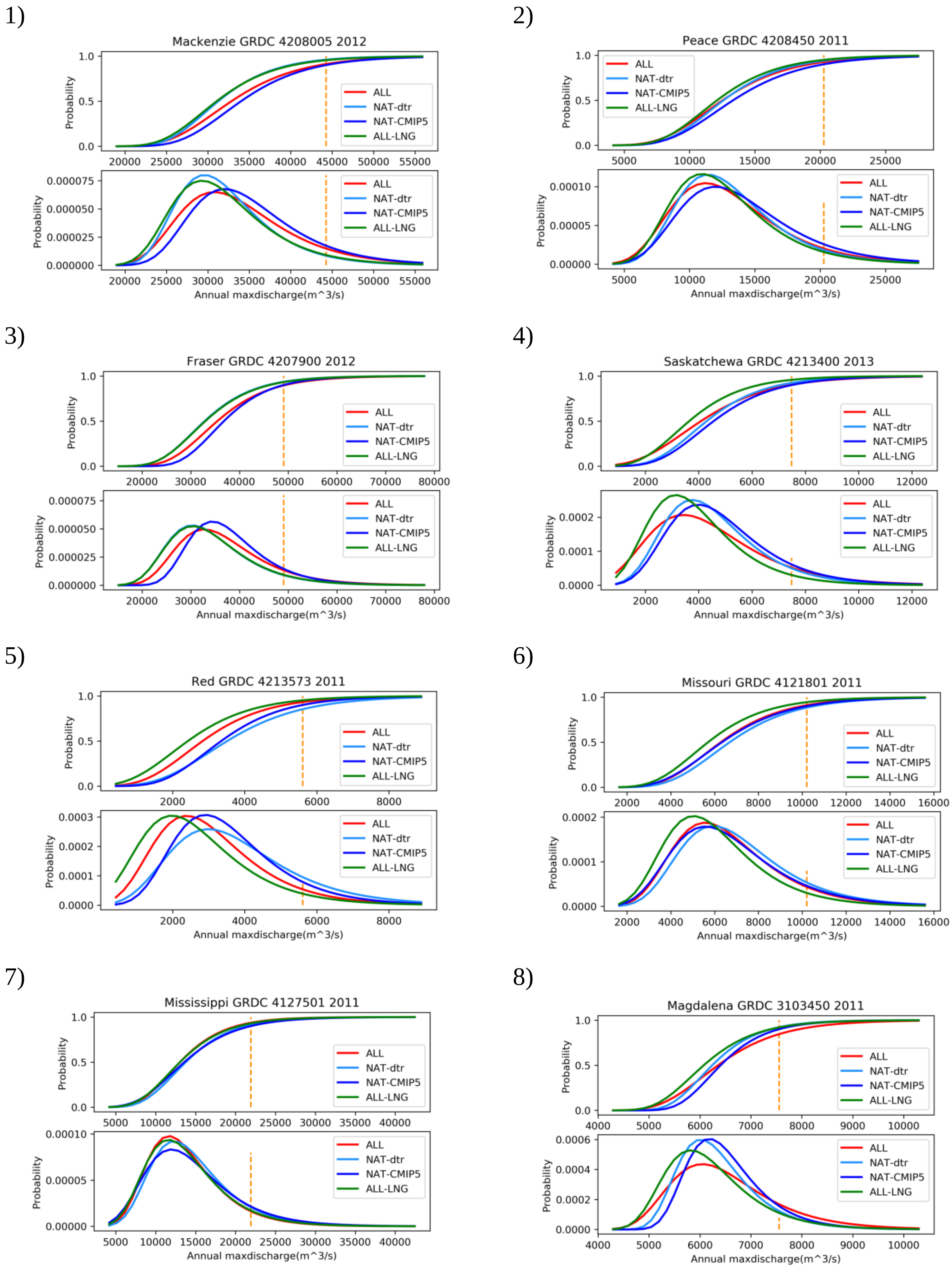

Fig. S6 The probability density function and cumulative distribution function of annual maximum daily discharge for 22 events derived from event attribution experiments (ALL, ALL-LNG, NAT-dtr, and NAT-CMIP5). The orange dot line indicates magnitude of 10-year flood in ALL-LNG experiment.

9)

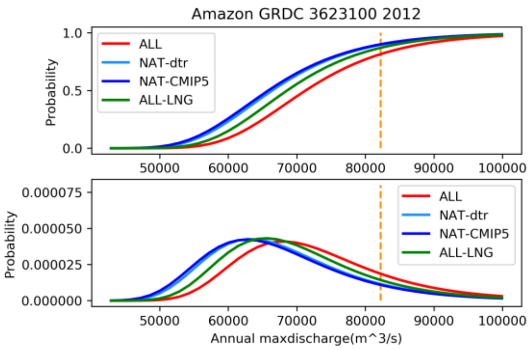

10)

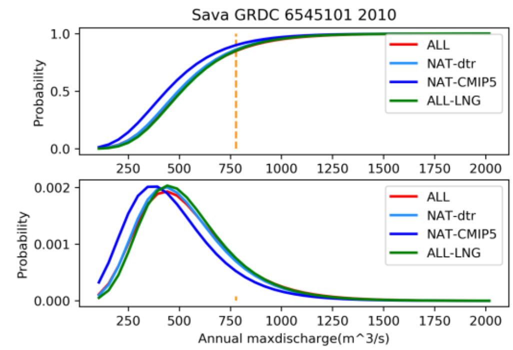

11)

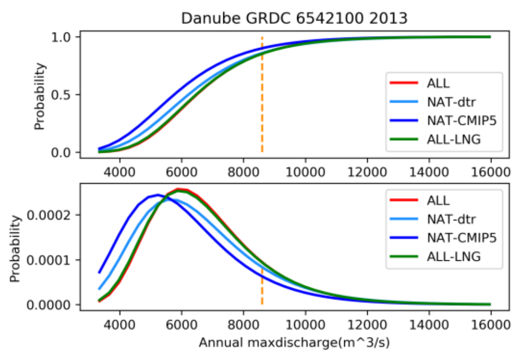

12)

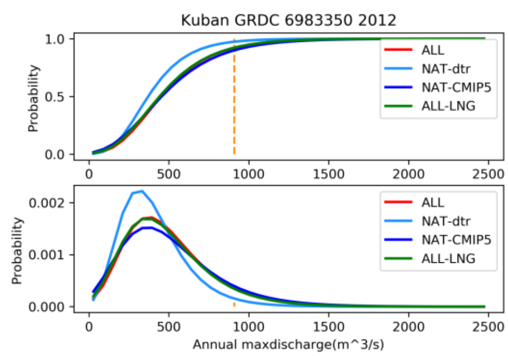

13)

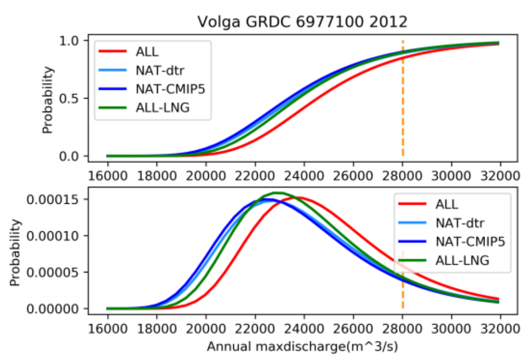

14)

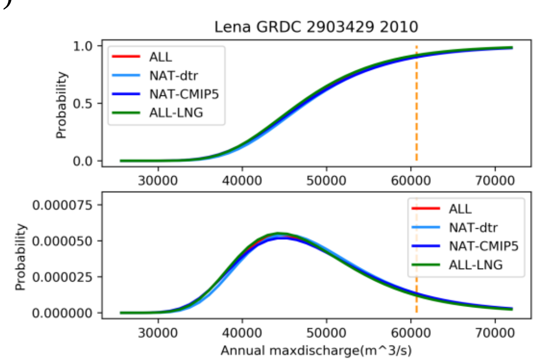

15)

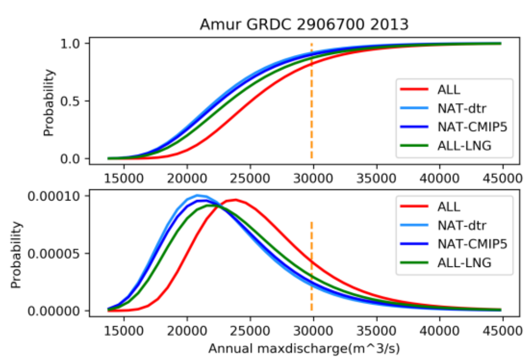

16)

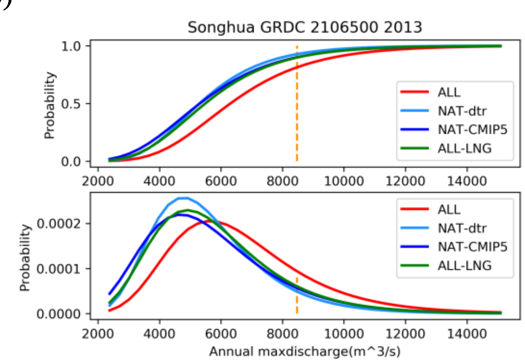

Fig. S6 The probability density function and cumulative distribution function of annual maximum daily discharge for 22 events derived from event attribution experiments (ALL, ALL-LNG, NAT-dtr, and NAT-CMIP5). The orange dot line indicates magnitude of 10-year flood in ALL-LNG experiment (continue).

17)

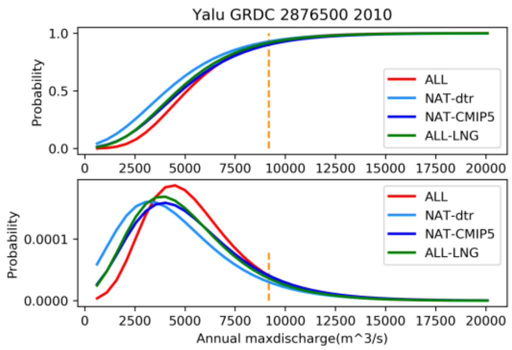

18)

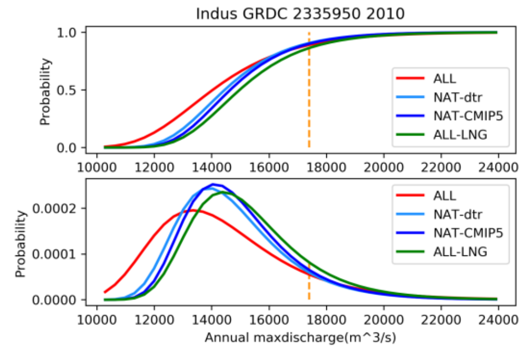

19)

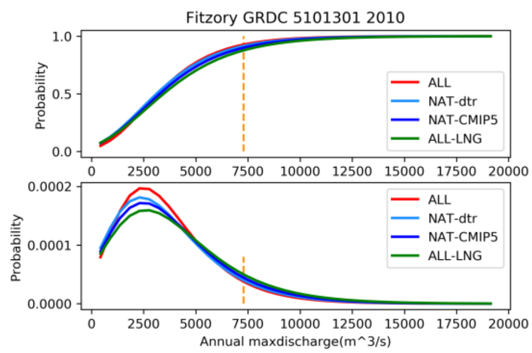

20)

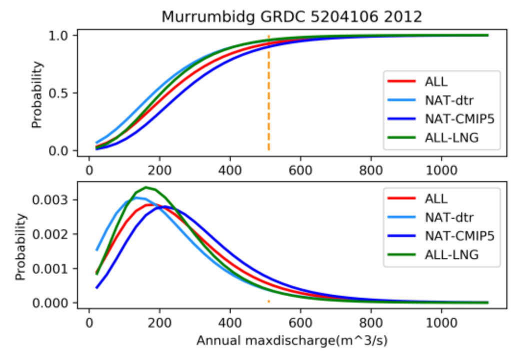

21)

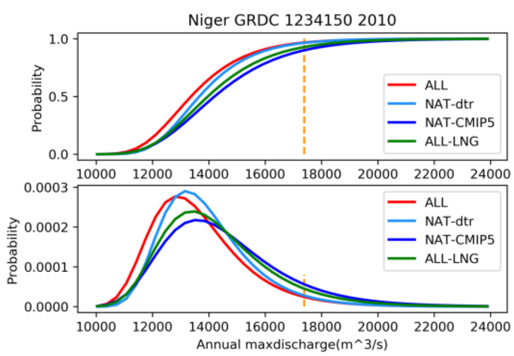

22)

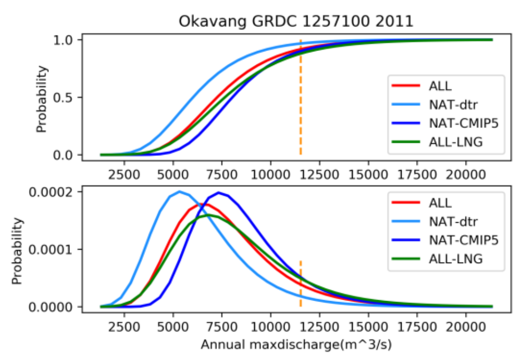

Fig. S6 Theprobability density function and cumulative distribution function of annual maximum daily discharge for 22 events derived from event attribution experiments (ALL, ALL-LNG, NAT-dtr, and NAT-CMIP5). The orange dot line indicates magnitude of 10-year flood in ALL-LNG experiment (continue).

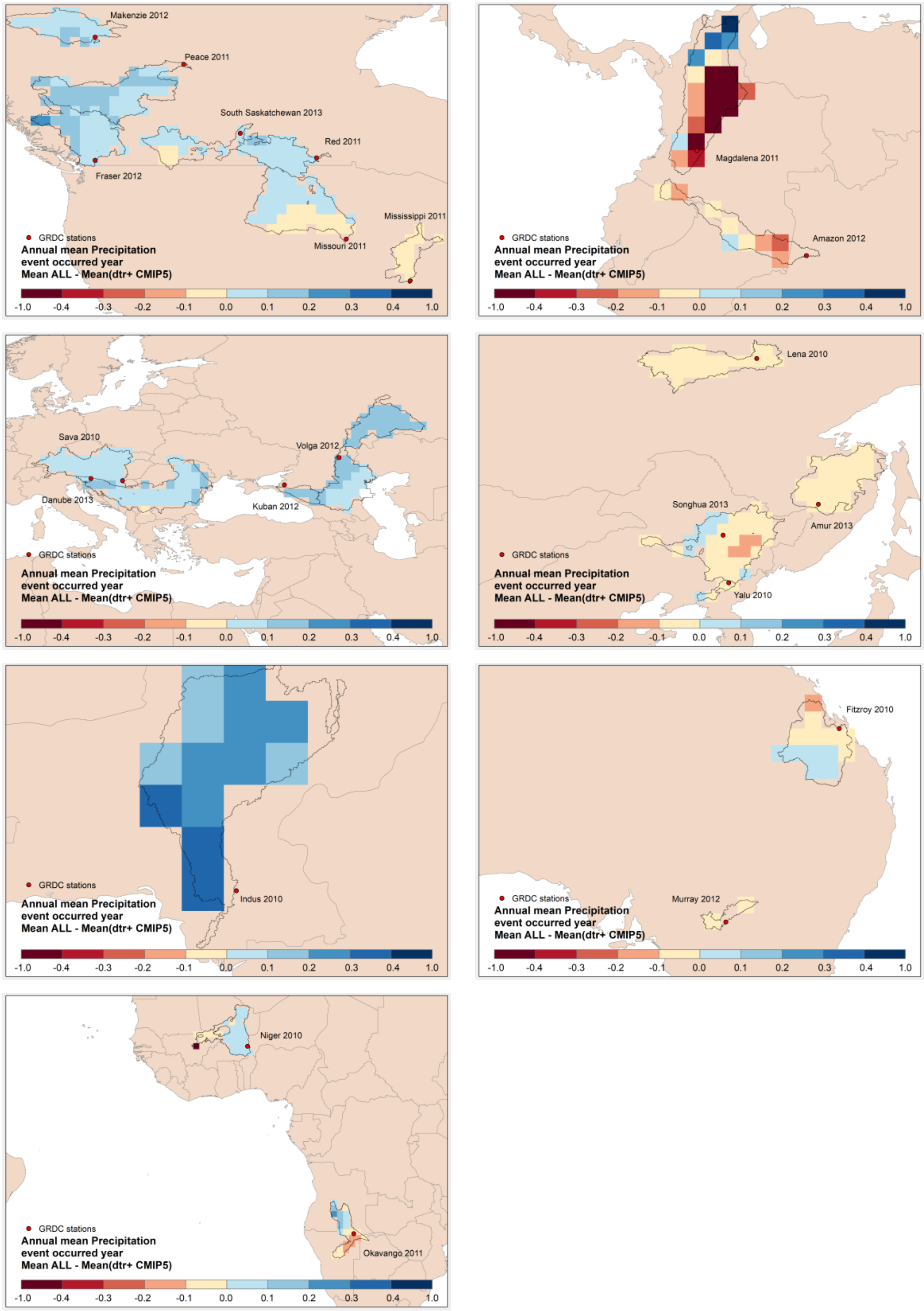

Fig. S7 Difference of average annual precipitation between ALL and mean of NAT (NAT-dtr and NAT-cmip5) experiments for selected flood events (mm/day).

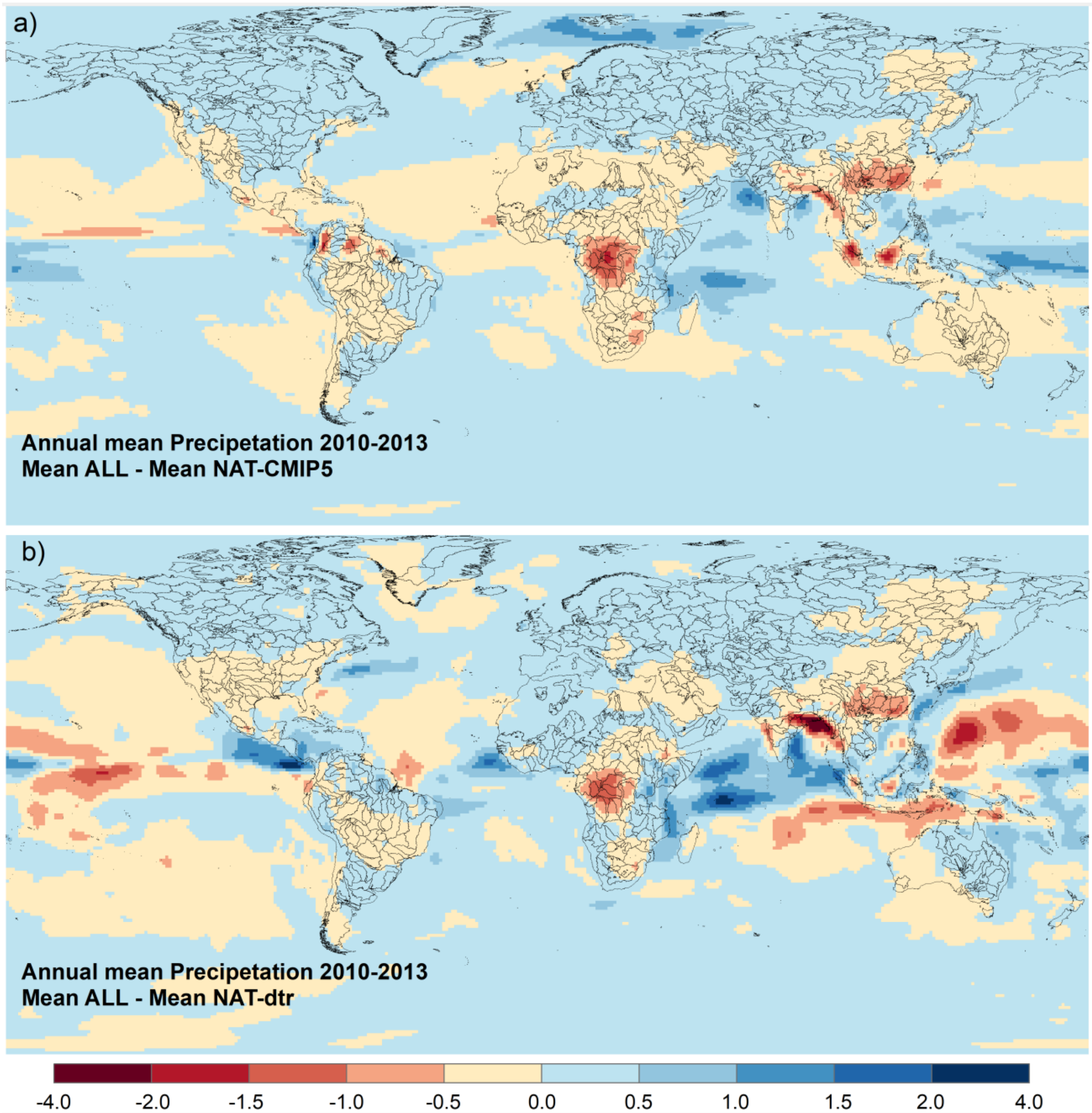

Fig. S8 Same for Fig. 3 but the difference between ALL and NAT-cmip5 (a) and ALL and NAT-dtr (b).

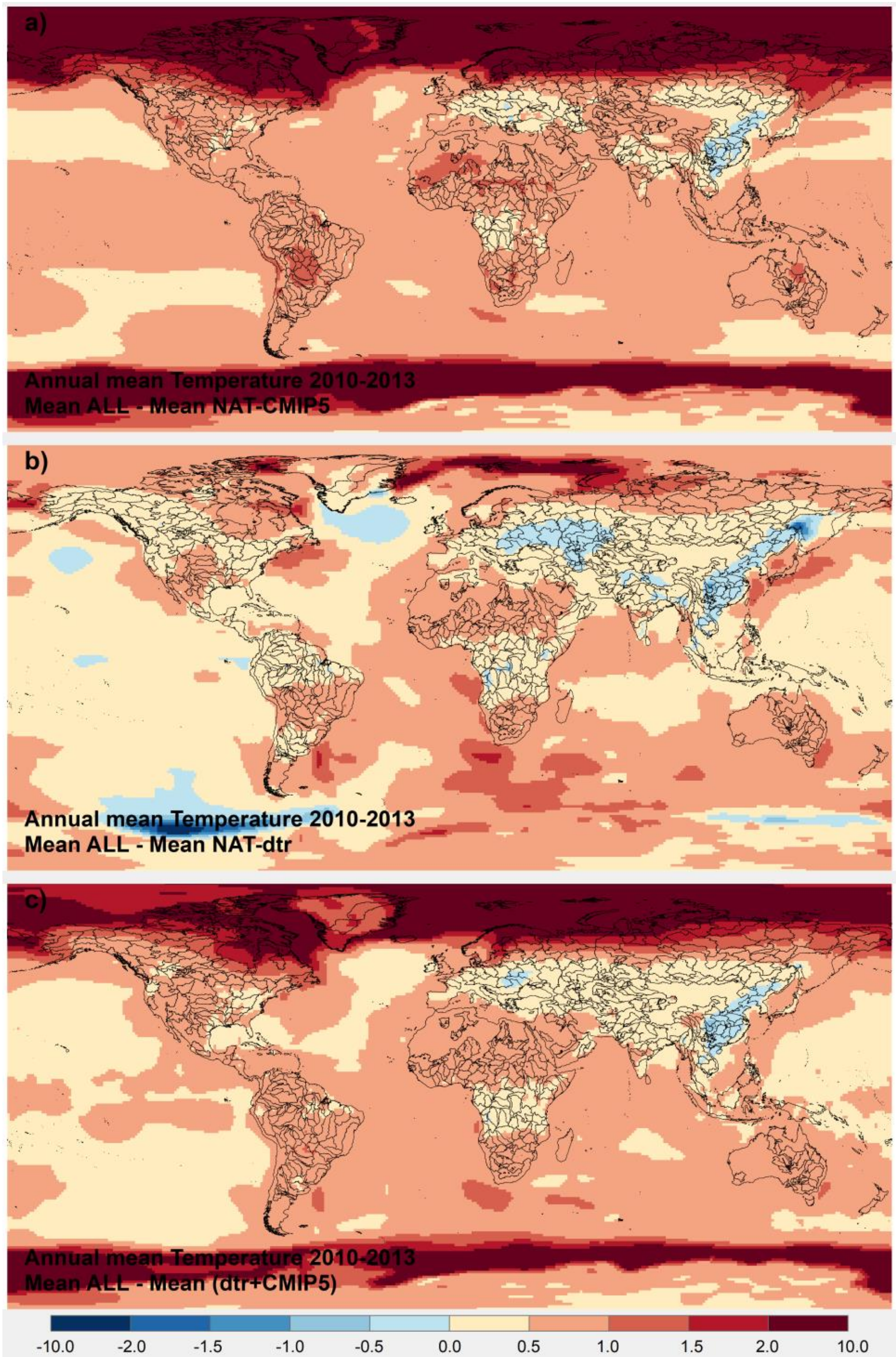

Fig. S9 Difference of average annual temperature (K). Difference between ALL and NAT-cmip5 (a), ALL and NAT-dtr (b), and ALL and NAT (average of NAT-dtr and NAT-cmip5) (c) experiments. Average for 2010-2013 are shown.

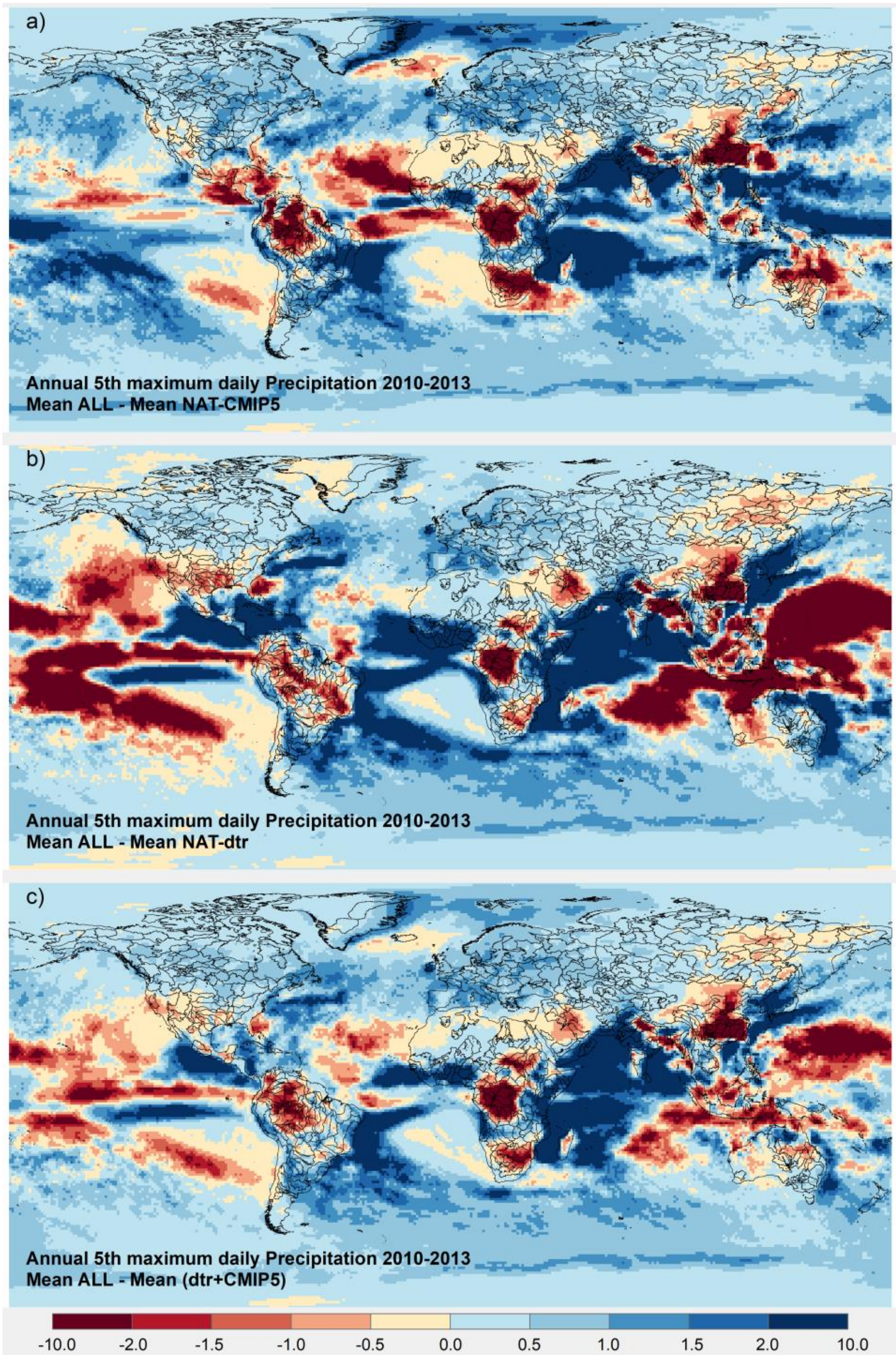

Fig. S10 Difference of mean annual 5th largest daily rainfall. Difference between ALL and NAT-cmip5 (a), ALL and NAT-dtr, and ALL and average of NAT-dtr and NAT-cmip5 experiments for 2010-2013 are shown.